

# A Slant Total Delay Observation Operator for the ICON and the COSMO Numerical Weather Models

Michael Bender<sup>1</sup>, Andreas Rhodin<sup>1</sup>, Harald Anlauf<sup>1</sup>, Christoph Schraff<sup>1</sup>, Klaus Stephan<sup>1</sup>, and Roland Potthast<sup>1,2</sup>

<sup>1</sup> Deutscher Wetterdienst, Frankfurter Str. 135, 63067 Offenbach, Germany.

<sup>2</sup>Department of Mathematics and Statistics, University of Reading, Whiteknights, PO Box 220, Berkshire RG6 6AX, UK

May 30, 2016

## Abstract

GPS slant total delays (STDs) are expected to provide valuable spatially resolved humidity information for numerical weather prediction. To take advantage of these data the German Weather Service (DWD) developed an STD observation operator for the global numerical weather model ICON and the local model COSMO-DE. The operator has interfaces to the En-VAR assimilation system of ICON and the local ensemble transform Kalman filter (LETKF) of COSMO. The delay is obtained by integrating the refractive index along the curved signal path which is estimated by a raytracer. The raytracer makes use of Fermat's principle to find the path of least travel time between the satellite and the ground receiver. The components of the operator and their interplay are described and a comprehensive study of its quality is presented.

The STD operator was validated using one month of STD and zenith total delay (ZTD) observations and operational model analyses from March 2015. Analyzing the observation minus model differences mapped to the zenith a bias of 10.1 mm and a standard deviation of 10.8 mm was found for ICON. For COSMO-DE the bias was 5.5 mm and the standard deviation was 10.0 mm. In both cases all observations with relative differences of less than 1.5 % to the model analysis were used. The mean relative differences were almost constant for all elevations indicating that the operator can be used down to very small elevations  $< 5^\circ$ .

## 1 Introduction

Microwaves propagating through the Earth's atmosphere are modified in a way which depends on the current atmospheric state. For most technical applications such modifications have undesirable effects but if these effects are well understood they provide a tool for atmosphere sounding. GNSS signals are modulated in a way which is optimal for positioning but also for estimating the exact travel time through the atmosphere. The signal travel time in the neutral atmosphere, i. e. the part of the atmosphere below the ionosphere reach-

ing up to  $\sim 100$  km, provides valuable information about weather patterns especially in the lower troposphere.

Up to now the GNSS zenith total delay (ZTD), i. e. the signal delay as compared to undisturbed propagation through vacuum in zenith direction, is the most widely used GNSS atmospheric product. ZTD observations are assimilated into the numerical weather models of many weather services and lead to improved weather forecasts. A small but positive impact was reported by [Mahfouf u. a. \(2015\)](#) and [Bennitt u. Jupp \(2012\)](#). Assimilation of the vertically integrated water vapor (IWV) is an

other option and comparable results were obtained (Kawabata u. a., 2007, 2011). The current state of the European GNSS atmosphere processing and GNSS data assimilation is reviewed by Guerova u. a. (2016).

The ZTD is integrated along the vertical axis and thus cannot provide information about the vertical structure of the atmosphere. It is therefore desirable to use other GNSS derived atmospheric products which do offer spatially resolved information about the atmosphere. The most promising quantity is the slant total delay (STD), i. e. the signal delay along a specific satellite – receiver path. GPS receivers usually track 8 – 12 GPS satellites simultaneously and the atmospheric state is scanned in different directions and at different elevations. Currently, most geodetic agencies replace GPS receivers with multi GNSS receivers which can track all visible satellites from most active satellite positioning systems, like GPS, GLONASS, BeiDou, Galileo and others. In the near future more than 100 satellites will be operating and more than 30 will be visible at any time. Within dense networks of ground-based GNSS receivers this leads to a large number of observations which scan the atmosphere from all directions, with a high temporal resolution and under all weather conditions. If STD observations of large GNSS networks are assimilated into numerical weather models where they are combined with a physical atmosphere model and a large number of other observations, it can be expected that the spatial structure of the model state will be improved (Ha u. a., 2003; Kawabata u. a., 2013). Especially the vertical structure of the atmospheric humidity is expected to improve as STDs are sensitive to humidity.

To utilize GNSS STDs was already suggested in an early stage of GNSS atmosphere sounding (Rocken u. a., 1993; Bevis u. a., 1992; Ware u. a., 1997) but first STD assimilation experiments started much later. There are two main reasons why the assimilation of STDs into numerical weather models is up to now not operational: (1) The processing of STDs with sufficient quality is much more sophisticated than the ZTD processing and most GNSS processing centers do not yet provide STDs. (2) The development of an STD observation operator is rather complex as the signal delay is an integrated quantity which depends on several model variables. Furthermore, the signal

propagates through large parts of the model domain, especially for satellites at low elevations.

Attempts to derive slant delays were made by Alber u. a. (2000) who described a method for obtaining STD observations from double differences and by Flores u. a. (2000) for tomographic applications. Braun u. a. (2001) estimated slant wet delays for validation with water vapor radiometer data and de Haan u. a. (2002) compared GPS STD data with their model equivalents for the case of a cold front passage. Different strategies for STD data processing were developed for GNSS water vapor tomography, see Notarpietro u. a. (2011), Bender u. a. (2011) and references therein. The processing of slant delays is still a field of active research (Kačmařík u. a., 2012).

The first STD assimilation studies were reported by MacDonald u. a. (2002), Ha u. a. (2003), Liu u. a. (2006) and Liu u. a. (2007) who used simulated STD observations. Eresmaa u. Järvinen (2006) developed an STD operator for HIRLAM which has later been extended by a raytracing algorithm (Eresmaa u. a., 2008). This operator was used for first assimilation experiments with real STD observations (Järvinen u. a., 2007). The results were encouraging but gave also reason for a critical examination of the information about anisotropic atmospheric structures which can be expected from the slant delays (Eresmaa u. a., 2007). More recent results were presented by Zus u. a. (2012) and Kawabata u. a. (2013) which indicate that the assimilation of STDs has a higher impact than the assimilation of ZTDs and leads to better resolved and more realistic humidity fields.

The German Weather Service (DWD) operates the icosahedral non-hydrostatic global model (ICON) with a horizontal resolution of 13 km and 90 vertical levels up to 75 km (Zängl u. a., 2014). Over Europe ICON is running with an increased horizontal resolution of 6.5 km. The hybrid En-Var data assimilation combines 3D-Var and a static B matrix with a flow dependent model background error provided by a local ensemble transform Kalman filter (LETKF) (Fernández del Río u. a., 2015). The non-hydrostatic COSMO-DE model covers Germany with a horizontal resolution of 2.8 km and 50 vertical levels up to 22 km. The operational COSMO-DE version runs with a nudging assimilation system, an ensemble Kalman filter for convective scale data assimilation (KENDA)

which is based on the LETKF is in a preoperational state (Schraff *u. a.*, 2016).

In order to take advantage of ground based GNSS atmosphere products the DWD developed an STD observation operator. Up to now no ground based GNSS data are operationally assimilated at the DWD. The STD operator was designed for the ICON global model and the COSMO-DE local model and can be called by the ICON En-Var assimilation system and the LETKF/COSMO system as well. After some basic definitions in Sec. 2 the operator implementation is described in Sec. 3. Sec. 4 provides a brief description of the interfaces to the assimilation systems and the validation of the operator with GNSS observations is described in Sec. 5.

## 2 Signal delays

The microwave signal transmitted by the GNSS satellites is delayed by the Earth's atmosphere. The delay due to the neutral atmosphere, i.e. the slant total delay (STD), can be estimated by GNSS processing systems and is defined by the optical path length  $L$  minus the geometric distance  $G$  between the satellite and the receiver (Bevis *u. a.*, 1992):

$$STD = L - G = \int_S n(s) ds - \int_G ds \quad (1)$$

The atmospheric refractive index along the signal path  $S$  is given by  $n(s)$ . The refractive index  $n$  is often replaced by the refractivity  $N = 10^6(n - 1)$  leading to

$$STD = \int_S (n(s) - 1) ds + (S - G) = 10^{-6} \int_S N ds + (S - G)$$

The geometric delay  $S - G = \int_S ds - \int_G ds$  describes the extra path length due to ray bending. The latter is often neglected but this is not possible when implementing an STD observation operator.

The zenith total delay (ZTD) is a special case of the STD where the satellite is located in the zenith of a given station. The deviations of the signal path  $S$  from a straight line are related to horizontal atmospheric gradients which are much smaller than the vertical gradients and can be neglected.

A good approximation of the ZTD is given by

$$ZTD \approx 10^{-6} \int_S N ds \approx 10^{-6} \int_0^\infty N(h) dh \quad (2)$$

where  $h$  is the height above the GNSS station.

Regarding the definition of signal delays there is no difference between ZTDs and STDs with satellites in the zenith. However, STDs and ZTDs are processed in a different way and the term "ZTD" is not only related to equ. 2 but also to a processing strategy where a large number of GNSS observations is combined to a hypothetical zenith delay. The processing of individual GNSS observations leads to STDs and the rare cases where a satellite passes through the zenith of a GNSS station are usually also referred to as STDs (Gendt *u. a.*, 2004).

The refractivity  $N$  is related to the atmospheric quantities temperature  $T$ , pressure  $p$  and the partial pressure of water vapor  $e$ . Several empirical expressions for  $N$  at microwave frequencies were developed (Smith *u. Weintraub*, 1953; Thayer, 1974; Aparicio *u. Laroche*, 2011). Usually the Thayer formula is applied

$$N = k_1 \cdot \frac{p_d}{T} Z_d^{-1} + k_2 \cdot \frac{e}{T} Z_w^{-1} + k_3 \cdot \frac{3}{T^2} Z_w^{-1} \quad (3)$$

where  $p_d$  is the partial pressure of dry air and  $Z_d^{-1}$  and  $Z_w^{-1}$  are the compressibility factors of dry air and water vapor. Several sets of the empirical constants  $k_1, k_2, k_3$  were found by different authors (Bevis *u. a.*, 1994; Rieger, 2002). A different approach was suggested by Aparicio *u. Laroche* (2011). The impact of the refractivity coefficients on the assimilation of radio occultation profiles was analyzed by Healy (2011).

## 3 STD operator

A GNSS STD observation operator needs to evaluate equ. 1 for a given model state and a set of GNSS observations. The most natural way is to apply Fermat's principle to equ. 1 and to find the path of least travel time which is equivalent to the least path delay. With such an approach the impact of the model state on both the signal path and the signal delay is considered.

The geometrical properties of the problem are described by choosing a set of appropriate reference systems and the corresponding transformations between them. With such a general approach it can be avoided to introduce correction terms, e.g. for considering the curvature of the Earth. This is done by choosing an ellipsoidal reference frame and a transformation, e. g., between Cartesian coordinates on the signal path and ellipsoidal coordinates of grid points.

### 3.1 Coordinates, reference frames and geoid

The STD operator has to deal with several different reference frames and coordinates either because the observations are given in different coordinates or because the computations are most efficient in a certain reference frame. Here, the reference frames used by the operator are described below before the structure of the operator is discussed.

**Observations** The GNSS observations consist of two parts: The GNSS station coordinates describe the exact receiver position and the STD is provided together with the azimuth and elevation in the local horizon system of the receiver (fig. 1). The coordinates of GNSS stations are usually given as geographical coordinates, i.e. latitude  $\beta$  and longitude  $\lambda$  are given with respect to a reference ellipsoid, e.g. WGS84, the station height is the height above geoid or mean sea level. The GNSS observations are linked to different GNSS satellites, each satellite having a certain azimuth  $\phi$  and elevation  $\varepsilon$  in the local horizon system  $(x_h, y_h, z_h)$  of the GNSS station. The horizon system is defined by a tangent plane to the ellipsoid at the station position and is usually described by a left handed Cartesian system with its origin at the receiver position. The  $x_h$ -axis is pointing north, the  $y_h$ -axis is pointing west. The azimuth is the angle between the transmitter-receiver-axis and the  $x_h$ -axis, the elevation the angle to the  $x_h$ - $y_h$ -plane (fig. 2).

The elevation of a GNSS satellite is the angle between the satellite-receiver-axis and the local horizontal plane as computed by the GNSS processing software. It is not the incident angle of the electromagnetic wave at the GNSS antenna which

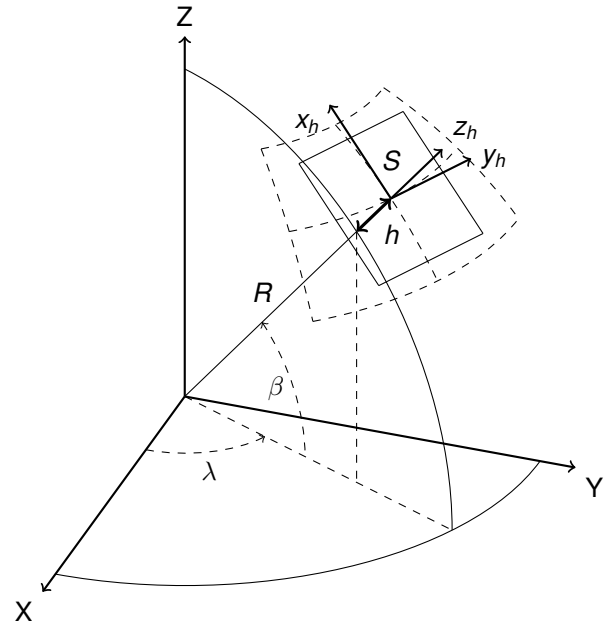


Figure 1: ECEF coordinates  $(X, Y, Z)$ , the corresponding ellipsoidal coordinates  $(\lambda, \beta, h)$  and the local horizon system  $(x_h, y_h, z_h)$  at the Station  $S$ .  $R$  is the geocentric radius of the Earth at latitude  $\beta$  and  $h$  is the station height above ellipsoid.

cannot be observed by GNSS receivers. The incident angle is always larger than the geometrical elevation of the transmitter and could be estimated by the raytracer but is not required by the STD operator. That applies to the azimuth too but the effect is much smaller.

As the satellite coordinates are usually not part of the meteorological data sets provided by the processing centers the satellite position has to be estimated using azimuth and elevation of the observed STD and the radius of the satellite orbit.

**Weather model** The reference frames used by numerical weather models are very often not well defined as latitude, longitude and height of the grid nodes are often given without specifying the reference frame. Consequently there is some freedom in interpreting these coordinates. Within this work it is assumed that the model frame is an ellipsoidal frame with heights above geoid, i.e. geographical coordinates.

**GNSS signal propagation** On its way from the GNSS satellite to the GNSS ground receiver the microwave signal propagates through vacuum, the ionosphere and the neutral atmosphere and is bent toward the direction of increasing refractive index. However, the deviation from a straight line ( $< 1000$  m) is small as compared to the distance between satellite and receiver ( $> 22000$  km) and it is most convenient to describe the signal propagation in a Cartesian reference frame  $(x, y, z)$  which is aligned to the satellite-receiver-axis (fig. 2). The  $x$ -axis is pointing from the receiver to the satellite and the  $z$ -axis is chosen to lie in a plane defined by the center of the Earth, the GNSS station and the satellite. The  $y$ -axis is chosen to obtain a right handed orthogonal system. Such a system can be obtained by rotating the basis vectors of the local horizon system by azimuth and elevation.

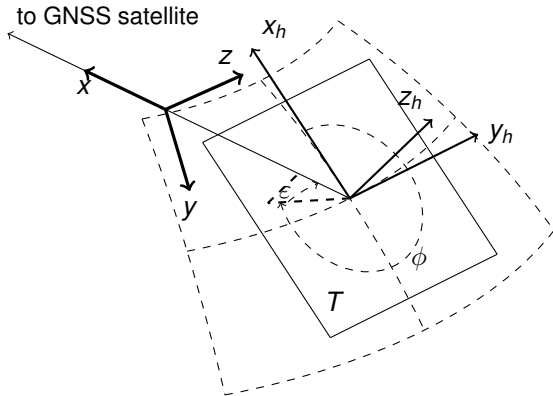


Figure 2: Azimuth  $\phi$  and elevation  $\epsilon$  of the GNSS satellite are defined with respect to the local horizon system  $(x_h, y_h, z_h)$  at the receiver position  $(\lambda, \beta, h)$ , i. e. the tangent plane  $T$  to the ellipsoid at the station (see fig. 1). The signal path is described in a reference system  $(x, y, z)$  which is aligned to the satellite-receiver-axis.

The vertical axis through the GNSS station is always in the  $x - z$ -plane of the signal propagation system and the  $y$ -axis is always perpendicular to the vertical axis. If the curved signal path is de-

scribed in such a reference system it is guaranteed that the strong vertical gradients have an impact only on the  $z$ -coordinate while the  $y$ -coordinate is defined by horizontal gradients (see sect. 3.4).

**Earth centered Earth fixed Cartesian coordinates** It would be rather laborious to define transformations between any pair of reference frames which are used while the transformations to Cartesian coordinates can be found in most textbooks about GNSS or geodesy (Hofmann-Wellenhof u. a., 2008; Xu, 2007). The most suitable Cartesian system is the Earth centered Earth fixed system (ECEF) which is fixed to the rotating Earth and where the station coordinates are not time dependent. The origin of the ECEF system is the center of the Earth, the  $X$ -axis is defined by the Greenwich meridian, the  $Z$ -axis by the rotation axis of the Earth and the  $Y$ -axis points east. All transformations which are not directly related to the ECEF system can be done in two steps: 1) Transformation to ECEF coordinates and 2) to the desired system.

This is not possible for geographical coordinates where the height is defined with respect to the geoid. Geoid corrections need to be applied which provide the height above ellipsoid which can easily be transformed.

**Geoid** The geoid is an empirical quantity which is related to the local gravity field of the Earth. There are different data sets which provide the geoid undulation and which can be used to turn the height above geoid into a height above ellipsoid. In this work the EIGEN-6c3stat geoid (Förste u. a., 2013) with a resolution of  $0.1^\circ$  was used for COSMO and the EGM96 geoid (Lemoine u. a., 1998) with a resolution of  $0.5^\circ$  was used for ICON. Geoid corrections were applied to the GNSS station heights and the heights of the model grid nodes in order to obtain ellipsoidal coordinates.

### 3.2 Geometrical setup

The geometry of the problem is basically defined by the satellite and receiver positions. The connecting line is already a good approximation of the signal path and is the starting condition for the iterative Newton solver used by the raytracer. The first

task of the STD operator is to define a straight line between satellite and receiver, i.e. the  $x$  axis in fig. 2. The satellite coordinates are usually not available and the azimuth and elevation of the given STD in the local horizon system of the GNSS station need to be used to estimate a vector pointing to the satellite. The mean radii of the satellite orbits are used to estimate the distance to the satellite. This is not a precise procedure and leads to errors of some kilometers in the satellite position especially if the azimuth and elevation angles are given with limited precision. However, the STD is dominated by the lower part of the atmosphere and the impact of this error on the signal path inside the model domain ( $< 75$  km) is negligible.

The connecting line is described in ECEF coordinates and a number of supporting points is defined on that line. These supporting points will be used by the raytracer and the numerical integration of the STD as well and their locations should be chosen well in order to obtain numerically stable results with a minimum number of points. For distributing the supporting points the line is divided in three parts: The most important lower part is located inside the model domain, the second part reaches up to a height  $h_{\max}$  between 100 km and 200 km which needs to be considered because of its contribution to the STD and the last part between  $h_{\max}$  and the satellite is assumed to be in vacuum and no supporting points are required here. However, the last point at the satellite position is always required and cannot be omitted without changing the signal path significantly. The impact of the ionosphere is completely neglected as the processing of the STD is based on an ionosphere-free combination which provides the delay due to the neutral atmosphere.

In COSMO all STDs which do not reach the model top while propagating through the COSMO domain are rejected. Any horizontal extrapolation of the model fields would introduce unnecessary uncertainties and would lead to inaccurate STDs. Regarding the large number of GNSS observations available for Germany (see section 5.1) the few STDs lost at the horizontal model boundaries can be neglected.

The number of supporting points can be chosen independently for the model domain ( $N_1$ ) and the region above the model top ( $N_2$ ).  $N_i$ ,  $i = 1, 2$ , is the minimum number of points for zenith direction

which is automatically scaled by  $\sin^{-1} \varepsilon$  for slants at lower elevations  $\varepsilon$ . The vertical distribution decreases with the atmospheric density and is scaled by an exponential law with scale heights  $H_i$ :

$$n(h) = n_0 \exp \left\{ \frac{h}{H_i} \right\} \quad (4)$$

The supporting points are placed where

$$h_j = -H_i (\ln n_j - \ln n_0) \quad (5)$$

with equidistant  $n_j = n_0 + j \cdot \Delta n$ ,  $j = 0, \dots, N_i - 1$  and  $\Delta n = (n(h_{\max}) - n_0)/(N_i - 1)$ . For the lower part of the slant inside the model domain good results were obtained with  $H_1 = 6500$  m and  $N_1$  comparable to the number of vertical model layers (COSMO-DE:  $N_1 = 50$ , ICON:  $N_2 = 90$ ). For the region above the model top a much larger scale height should be chosen, e.g.  $H_2 = 40000$  m, but the number of points might be quite small, e.g.  $N_2 \leq 20$ .

The supporting points computed in this way are not related to the model grid and it can in general not be guaranteed that each horizontal grid layer or each grid cell along the signal path is regarded. However, computing intersection points between the signal path and some grid layers can lead to a very inhomogeneous distribution of supporting points on the signal path, especially at low elevations. The algorithm described above should work equally well if  $N_1$  is sufficiently large and the scale height  $H_1$  is chosen well.

After the 3D coordinates of the supporting points are determined the model grid nodes which contribute to the STD can easily be identified (see section 4).

### 3.3 Interpolation and extrapolation

For estimating the STD the refractive index must be known along the signal path, i. e. at the supporting points, and spatial interpolation between the grid nodes is required. In this work an interpolation procedure was chosen which works equally well with ICON and COSMO. In a first step the refractivity  $N$  is computed at the model grid nodes surrounding the reference point. The vertical interpolation within the grid columns provides  $N$  at the reference height and a bilinear horizontal interpolation leads to the final interpolated value on the signal path.

The refractivity  $N$  is computed using equ. 3 with the refractivity coefficients given by [Bevis u. a. \(1994\)](#):  $k_1 = 77.60 \text{ K hPa}^{-1}$ ,  $k_2 = 70.40 \text{ K hPa}^{-1}$  and  $k_3 = 3.739 \cdot 10^5 \text{ K}^2 \text{ hPa}^{-1}$ . An ideal gas is assumed and the compressibility factors are set to 1, i. e.  $Z_{d,w}^{-1} = 1$ . The choice of the refractivity coefficients has a large impact on the computed delays and more detailed studies are required to identify the optimal way for computing  $N$  ([Healy, 2011](#); [Aparicio u. Laroche, 2011](#)).

It is assumed that the refractivity decreases almost exponentially with increasing height and can be interpolated by

$$N(z) = N_2 \cdot \left( \frac{N_1}{N_2} \right)^{\left( \frac{h_2 - z}{h_2 - h_1} \right)}, \quad (6)$$

where  $N_1 = N(h_1)$  is the refractivity at the lower grid node and  $N_2 = N(h_2)$  is the refractivity at the upper node,  $h_2 > h_1$ .  $N(z)$  is the interpolated refractivity at the height  $z$ ,  $h_1 \leq z \leq h_2$ .

For horizontal interpolation the grid nodes at the corners of the cell containing the reference point are used, i. e. 4 nodes in case of rotated latitude/longitude grid of COSMO-DE and 3 nodes in case of the icosahedral-triangular ICON grid. The refractivity at the reference point is obtained by bilinear interpolation between the surrounding corners where the vertically interpolated refractivity was computed in the previous step. With some minor modifications the same bilinear interpolation algorithm can be used to interpolate between 3 and 4 nodes.

The refractivity field inside the model domain accounts for the major part of the STD but there is a small contribution from the atmosphere above the model top layer which cannot be neglected. For COSMO-DE with the model top at 22 km the contribution to the ZTD is about 10 cm. The most convenient way is to use the Saastamoinen model ([Saastamoinen, 1972](#); [Elgered u. a., 1991](#)) which provides the ZHD above a given altitude, e. g. the model top. This is a reliable way for correcting the model ZTDs and the ZHD mapped to the signal path is also used to improve model STDs ([Eresmaa u. Järvinen, 2006](#)). However, the atmosphere above the model top does not only provide an additional contribution to the STD but does also affect the whole signal path, i. e. the incident angle and the height of the path. Small variations of

the signal path inside the model domain can lead to rather large variations of the corresponding delay. These variations cannot be corrected by the mapped Saastamoinen ZHD and strategies for estimating the refractivity profile above the model top need to be developed.

The STD operator provides three options for extending the vertical profile: exponential vertical extrapolation, the MSIS empirical atmosphere model ([Picone u. a., 2002](#)) and the U.S. standard atmosphere, 1976 ([NOAA, 1976](#)).

The refractivity profile can easily be extrapolated to any height using equ. 6 and the two topmost layers of the model column containing the last supporting point inside the model domain. This leads to satisfactory results for ICON which reaches up to 75 km but to rather large errors of  $\approx 1$  cm for COSMO-DE which is limited to a height of 22 km. By extrapolating the refractivity assumptions about the temperature and pressure profiles are made. In case of COSMO-DE the temperature profile within the lower stratosphere is extrapolated up to 100 km – 200 km and the temperature variations in the mesosphere and thermosphere are neglected.

Much better results could be expected if realistic temperature and pressure profiles were used. The NRLMSISE-00 empirical model ([Picone u. a., 2002](#)) of the atmosphere provides temperature and pressure profiles for any given position and time up to the altitude of satellite orbits. The delays obtained with these data are close to the Saastamoinen delays and lead to good results. However, corrections based on climatological data are not related to the current atmospheric state.

Another option to obtain vertical profiles is the U.S. standard atmosphere, 1976, which provides a profile based on temperature lapse rates for different altitudes. This temperature profile can easily be adapted to any available model profile by continuing the model temperatures with the predefined temperature lapse rates. The pressure profile of the standard atmosphere makes use of the temperature profile and is adjusted automatically. However, for extending the pressure profile above 86 km the number densities of individual gas species need to be computed which is rather complex. Instead, the pressure levels tabulated in ([NOAA, 1976](#)) are used to interpolate the pressure based on equ. 6 leading to a fixed pressure pro-

file above 86 km. This approach seems to give the best results with COSMO-DE and was used to compute the data provided in Sect. 5.

### 3.4 Raytracing

A detailed description of the raytracing algorithm and its performance is available (Zus u. a., 2012, 2013; Nafisi u. a., 2011) and only a short introduction is given here. One way to estimate the signal path in optical media is to apply Fermat's principle, i.e. to minimize the optical path length  $L = \int_S n ds$ . This leads to a variational problem which can most easily be described in a reference frame with the  $x$  axis pointing from the receiver to the satellite, i.e. the slant system described in sect. 3.1 and fig. 2. The signal path is described by the deviations from a straight line  $y(x)$  and  $z(x)$  which are functions of the independent variable  $x$ :

$$L = \int_a^b n(x, y(x), z(x)) \cdot \sqrt{1 + y'(x)^2 + z'(x)^2} dx \quad (7)$$

Here,  $y'$  and  $z'$  are the derivatives with respect to  $x$ . In this form only two dependent variables  $y$  and  $z$  need to be estimated. After the curved signal path  $S = (x, y(x), z(x))$  was determined equ. 7 provides a way to compute the STD along any curved path. Using the Euler-Lagrange-Equations the variational problem can be converted into a set of differential equations (Courant u. Hilbert, 1953):

$$y'' = \left( \frac{n_y}{n} - \frac{n_x}{n} y' \right) (1 + y'^2 + z'^2) \quad (8)$$

$$z'' = \left( \frac{n_z}{n} - \frac{n_x}{n} z' \right) (1 + y'^2 + z'^2) \quad (9)$$

where  $n_x = \frac{\partial n}{\partial x}$ ,  $n_y = \frac{\partial n}{\partial y}$  and  $n_z = \frac{\partial n}{\partial z}$ . These equations have to be solved for the boundary conditions

$$y(a) = z(a) = y(b) = z(b) = 0 \quad (10)$$

with the receiver being at  $x = a$  and the satellite at  $x = b$ .

To solve the two coupled differential equations a set of supporting points along the  $x$  axis was defined in sect. 3.2. The curve between these points is approximated by Lagrange polynomials which can be differentiated by differentiating the Lagrange basis polynomials.  $y'$ ,  $y''$ ,  $z'$  and  $z''$  are

replaced by the derivatives of the Lagrange polynomials and the differential equations become a set of  $2(N_1 + N_2) - 2$  nonlinear algebraic equations,  $N_1 + N_2$  being the total number of supporting points. Such a set of non-linear equations can be solved by Newton's algorithm but requires their Jacobians. The third derivatives of the Lagrange polynomials can easily be obtained. The computationally most expensive part are the derivatives  $n_x$ ,  $n_y$  and  $n_z$  as  $(x, y, z)$  of the Cartesian slant system depend on  $(\lambda, \beta, h)$  in the ellipsoidal system and three transformations are required: ellipsoidal system  $\Leftrightarrow$  ECEF  $\Leftrightarrow$  local horizon system of the GNSS station  $\Leftrightarrow$  slant system. The Jacobians of these transformations are required to obtain the derivatives of  $n$  and their Hessians to solve Newton's algorithm.

This iterative algorithm provides estimates of  $y_k = y(x_k)$  and  $z_k = z(x_k)$ ,  $x_k$  being the supporting points on the  $x$  axis. After some iterations a good estimate of the curved signal path  $S = S(x_k, y(x_k), z(x_k))$ ,  $k = 1, \dots, N_1 + N_2$  is obtained. Practically, the Newton algorithm converges very fast to a stable solution as the straight line is already a rather good approximation. In the NWP framework deviations  $y$  and  $z$  of several hundred meters over distances of several thousand kilometers are found. Under these conditions one or two iterations are sufficient for elevations  $\geq 3^\circ$  (Zus u. a., 2012).

### 3.5 Numerical integration

The STD (equ. 1) is the integral of the refractive index along the signal path. Numerically this is a weighted sum of the refractive index defined on a set of supporting points along the signal path. The processing time increases with the number of supporting points and an efficient integration algorithm which provides a good estimate of the integral with a minimum of supporting points should be chosen. In this work a cubic four point interpolation of unequally spaced data was used (Gill u. Miller, 1972).

The integration along the curved signal path is given by equ. 7. The functions  $y(x)$ ,  $z(x)$  and their derivatives  $y'(x)$ ,  $z'(x)$  were already estimated by the raytracing algorithm and equ. 7 is just a 1-dim integral to be evaluated at the same set of support-

ing points  $x_k$  already used by the raytracer.

## 4 Assimilation system and MPI interface

The STD operator was designed independently from the model or the assimilation system in order to run with the global ICON/En-Var and the regional COSMO LETKF as well. As the GNSS signals propagate through rather large parts of the models it is important to define a general interface which provides all relevant information to the STD operator. These data need to be sufficient to estimate the curved signal path and the slant delay as well without any further access to the model fields. To meet these requirements the STD operator was split into two parts which are called by driver routines. All necessary interprocessor communication is done by the driver routines which need to be implemented for each specific assimilation system. The STD operator doesn't contain any MPI/OpenMP calls.

The driver routine starts to read all GNSS observations from the assimilation time window and decides how to distribute the data across the processors in the MPI environment. After subsets of the observations have been copied to each processor the first part of the STD operator is called. The first part implements the geometrical setup for each single observation, i.e. it defines a straight line from the satellite to the receiver and a set of supporting points on that line as described in sect. 3.2. This can be done without any access to the model fields, only the observations are required. After all observations have been processed the driver routine reads the list of supporting points and computes the model columns in the vicinity of these points. Depending on the elevation and the height of the model top model data within a radius of  $\sim 200$  km (COSMO) or  $\sim 600$  km (ICON) need to be accessed. These model columns are requested from the processors holding the corresponding model subdomain. In an MPI exchange step all necessary data are copied to the corresponding processors. The second part of the STD operator gets access to the model columns in the vicinity of the supporting points. It calls the raytracer, does the interpolation and the numerical in-

tegration along the signal path and provides the simulated STD. As the signal path is not known in advance it is not sufficient to provide the model state only at the grid nodes surrounding the supporting points but parts of the grid columns extending up to  $\sim 1000$  m above the supporting points are required. In the last step the driver routine collects all observations and their model equivalents and transfers them to the assimilation system.

The most crucial part is the distribution of observations to processors as the processing time depends significantly on the STD elevation. For STDs with low elevations the station position becomes almost irrelevant as data from large parts of the model must be collected and the observations might be processed on any processor without increasing the data exchange considerably. However, for ZTD observations it might be beneficial to process the observation on the processor which holds the data of the required region. To improve the load balance at least the distribution of GNSS stations inside the model domain, the number of observations per station and the distribution of elevations must be considered. In the current implementation it is assumed that the computing time per STD can be scaled with a mapping function and the observations are distributed in order to achieve almost similar computing times on all processors. The positions of the GNSS stations are not yet regarded and observations of all stations are distributed uniformly to all processors. This leaves much room for improvements and further work is required.

## 5 Validation of the STD operator with observations

### 5.1 GNSS observations

Most European countries operate dense GNSS networks for geodetic applications. These networks do also provide valuable atmospheric information if the data are processed in an appropriate way. The EUMETNET GNSS Water Vapor Programme (E-GVAP, see <http://egvap.dmi.dk>) was started in 2005 as a cooperation of most European GNSS processing centers and weather services. One of the major achievements of E-GVAP

was the setup of an operational GNSS atmosphere processing system and many weather services started to assimilate GNSS ZTD data into their numerical weather models. Currently, the data of more than 2000 European stations are available in near real-time, i. e. hourly batches of data are provided with a delay of less than 30 minutes. The E-GVAP data set does also include global data, e. g. from the IGS network and data from northern America provided by NOAA.

The GNSS data are collected and processed on a national level and there exist considerable differences between the processing centers regarding the processing strategies, the software used and the derivation of atmospheric products. The temporal resolution of the products ranges from 5 min. to 60 min.

The development of improved STD processing techniques is currently an active field of research and many different approaches are investigated (Bender u. a., 2011; van der Marel u. Gündlich, 2006; Bi u. a., 2006; de Vries, 2006; de Haan u. a., 2002). For integrated atmospheric quantities like STDs no standard exists which could be used as a reference for different processing techniques and it is rather difficult to identify the best solution (Kačmařík u. a., 2012).

Up to now no STD data are distributed by E-GVAP. However, for Germany operational STD data are available from the GFZ in Potsdam. The observations of the German SAPOS network with more than 250 stations are processed together with some minor networks and stations from neighbored countries leading to hourly data sets of more than 60000 STDs (Bender u. a., 2011; Gendt u. a., 2004). The quality of the STD data was validated using water vapor radiometers running either in a hemisphere scanning mode or in GPS tracking mode (Shangguan u. a., 2015; Deng u. a., 2011; Bender u. a., 2008).

The E-GVAP and GFZ data sets are available at the DWD and were used for monitoring and validation studies.

## 5.2 Impact of ray bending

The ray bending in the atmosphere has a significant impact on the signal delay. The curved path is not only longer than the straight line between satel-

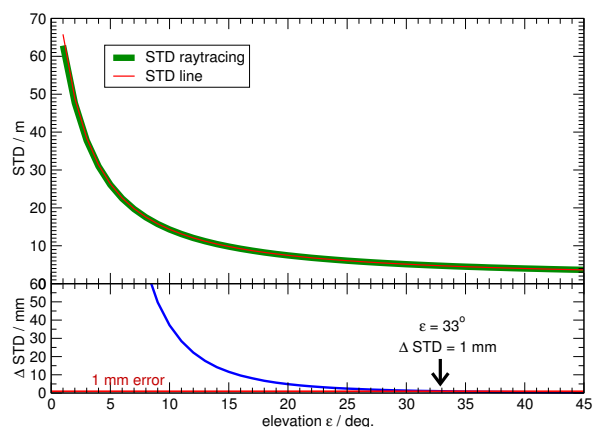


Figure 3: Impact of ray bending on the STD: The STD depending on the elevation computed for a curved signal path (green) and a straight line (red) is shown in the upper graph, the difference between both curves is shown in the lower graph (blue).

lite and receiver but always above this line. Consequently, the refractivity along the curved path is slightly smaller than along the straight line. This results in a systematically overestimated STD when integrating along the straight line. The effect is shown in fig. 3 where the signal delays were computed for a typical weather situation with and without raytracing. The STD increases in an almost linear way from about 2.3 m in zenith direction ( $\varepsilon = 90^\circ$ ) to  $\sim 3.6$  m at  $\varepsilon = 40^\circ$ . In this range the impact of the raytracing is negligible ( $\Delta_{\text{STD}} < 1$  mm). Below  $\varepsilon = 30^\circ$  the STD increases much faster and the contributions from the raytracing increase. At elevations below  $\sim 35^\circ$  ray bending cannot be neglected and leads to an error of about 35 mm at  $\varepsilon = 10^\circ$ . The STD observation error is usually below 0.5 %. If an observation error of  $\sim 75$  mm at  $\varepsilon = 10^\circ$  (0.5 % of  $\sim 15$  m) was assumed the effect of ray bending would exceed 50 % of the observation error. In case of more optimistic STD error estimates the effect would be even larger. To keep the operator error below 1 mm raytracing is required for elevations below  $\sim 35^\circ$ .

The curved signal paths estimated by the ray-tracer for elevations between  $1^\circ$  and  $30^\circ$  are shown in fig. 4. The functions  $z(x)$  and  $y(x)$  describe the deviations of the signal path from a straight line (see sect. 3.4) and  $x$  is the distance

to the GNSS receiver in the origin of the slant system (sect. 3.1, fig. 2). The deviations  $z(x)$  (fig. 4, top), i. e. in a plane containing the vertical axis, are dominated by the vertical gradient and can get as large as several hundred meters, e. g.  $\sim 250$  m at  $\varepsilon = 5^\circ$ . The deviations  $y(x)$  (fig. 4, bottom) in a horizontal plane are much smaller, i. e. do not exceed 1 m which is well below the resolution of numerical weather models and can be neglected.

Fig. 4 also demonstrates that the complete signal path inside the model grid is modified by ray bending. The green curves in fig. 4 (top) indicate the distances from the receiver where signal path reaches the model top layer (e.g. 20 km, light green and 40 km, dark green). The region left of the green curves indicates the model domain, on the right side the model state needs to be vertically extrapolated (see sect. 3.3). Even in case of a regional model which covers the atmosphere up to 20 km the maximum of  $z(x)$  is inside the model domain and the whole signal path is shifted upwards as compared to the connecting line. It is obvious that even small changes in the vertically extrapolated field can shift the maximum of  $z(x)$  and the signal path inside the model domain. As the section of the path inside the model domain can exceed 100 km the integrated effect becomes large which explains why the STDs integrated along the connecting line are always greater than the real delays even though the path length is somewhat smaller.

### 5.3 Validation with ICON

One month of operational ICON analyses from 1.3.2015, 0:00 UTC to 31.3.2015, 21:00 UTC was used to investigate the quality of the STD operator. ICON analyses are available every three hours beginning at 0:00 UTC, i. e. 8 model states were available per day. At that time ICON was running with a horizontal resolution of 13 km and no ground based GNSS data were assimilated. The STD operator was running in passive mode within the EnVar environment of ICON, i. e. the model equivalents of the STD and ZTD observations were computed for monitoring purposes but not assimilated. All GNSS data available within the 3 hour assimilation window were used.

For data validation the difference  $\Delta$  between the

observed STD and the simulated STD obtained with the STD operator was analyzed:

$$\Delta = STD_{\text{obs}} - STD_{\text{mod}} \quad (11)$$

The STD depends on elevation and the absolute differences  $\Delta$  grow with decreasing elevation. The differences of mapped STD data and the relative differences are therefore used to characterize large STD data sets. The difference  $\Delta_{\text{map}}$  between the STD data mapped to the zenith is given by

$$\Delta_{\text{map}} = m_{\text{MF}}^{-1} \cdot (STD_{\text{obs}} - STD_{\text{mod}}) \quad (12)$$

where  $m_{\text{MF}}$  is the mapping function. Another important quantity is the relative difference in %:

$$\Delta_{\text{rel}} = 100 \cdot \frac{(STD_{\text{obs}} - STD_{\text{mod}})}{STD_{\text{obs}}} \quad (13)$$

To describe the quality of the STD operator the mean difference  $\bar{\Delta}$  and the standard deviation  $\sigma$  of these quantities is computed for all stations and the whole data set. In case of ZTD data only the ZTD differences as in equ. 11 were analyzed.

The E-GVAP ZTD data set provides more than  $7.5 \cdot 10^6$  globally distributed ZTD observations for March 2015 which are processed by 11 GNSS processing centers. Some of them provide several alternative ZTD products leading to 18 different ZTD products in total. Within this work no attempts were made to distinguish between different products and all ZTD data were used to estimate the bias and standard deviation as shown in tab. 1, col. *all*. In a second step a first guess check was applied to restrict the differences to  $\Delta \leq 1.5\%$ , i. e. to  $\sim 35$  mm for a ZTD of  $\sim 2.3$  m. This constraint rejects about 2.4 % of the data and leads to an improved standard deviation  $\sigma = 11.9\%$  (col. *selected* in tab. 1). This is within the range of expected ZTD errors between 6 and 15 mm. The signal path in zenith direction is affected by horizontal gradients only and the impact of the raytracer is of the order of rounding errors. To save computing time the raytracer was switched off for elevations above a threshold of  $\varepsilon > 40^\circ$ .

The performance of the STD operator with respect to STD observations was validated using the GFZ data set which covers 312 stations in central Europe with a temporal resolution of 2.5 minutes. About  $44 \cdot 10^6$  STD observations were available for March 2015. Because of the higher temporal resolution this data set is much larger than

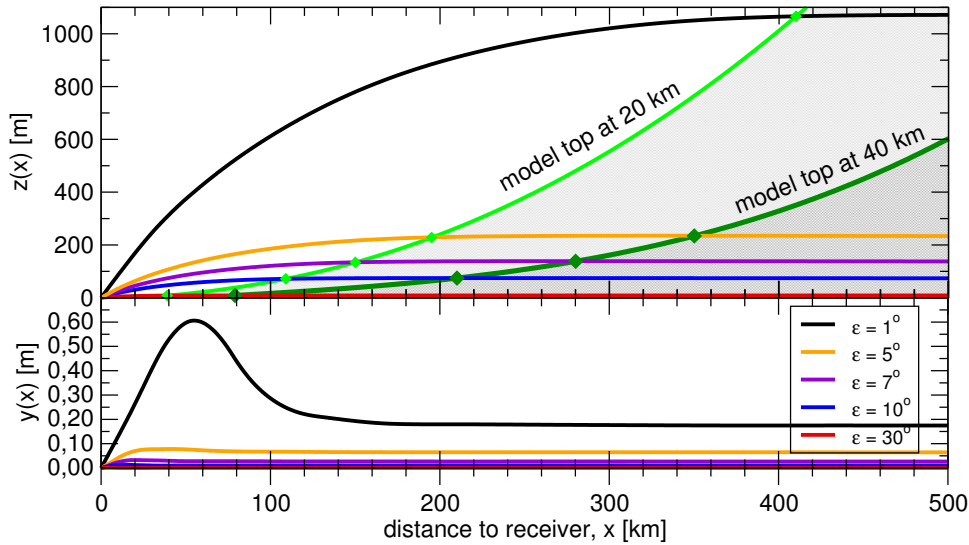


Figure 4: Signal path, deviations from a straight line. The three components of the signal path  $S = (x, y(x), z(x))$  are shown: The independent variable  $x$  is the distance to the GNSS receiver in km,  $z(x)$  (top) indicates the vertical deviation from a straight line in a plane containing the vertical axis and  $y(x)$  (bottom) indicates the horizontal deviation due to horizontal gradients only.  $z$  and  $y$  are given in meter. The green curves in the upper graph show the distance between the GNSS receiver and the model top for different elevations.

ICON	all	selected
$N_{\text{obs}}$	7679516	7496843
$\bar{\Delta}$ [mm]	1.6	2.0
$\sigma$ [mm]	16.6	11.9

Table 1: Verification of ZTD observations with ICON for March 2015.  $\bar{\Delta}$  and  $\sigma$  were computed using all data (col. *all*) or selected data with  $\Delta \leq 1.5\%$  (col. *selected*).

the ZTD data set. The results are given in tab. 2. As in case of the ZTD data the errors were computed using all data and using selected data with  $\Delta \leq 1.5\%$ , i. e.  $\sim 97.6\%$  of the original data. The bias  $\bar{\Delta}$  is quite large and is dominated by the rather large differences at low elevations.  $\bar{\Delta}$  depends on the distribution of elevations which changes considerably with geographic latitude. It is therefore a quantity which should not be used to characterize global data sets. Much more useful is the bias of the mapped differences  $\bar{\Delta}_{\text{map}}$  which can

also easily be compared to the ZTD bias. The STD bias  $\bar{\Delta}_{\text{map}}$  appears to be much larger than the ZTD bias, i. e. 10.6 mm to 1.6 mm for all data and 10.2 mm to 2.2 mm for the selected data. This is a well known feature of the GFZ data sets which are processed using relative antenna calibration instead of the absolute antenna calibration used by most other processing centers. This leads to an offset of about 6 mm. Such an offset is also present in the GFZ ZTD data but has a rather small impact on the bias in tab. 1 as the E-GVAP data set contains only  $\sim 8.5\%$  data from the GFZ.

The standard deviation  $\sigma_{\text{map}}$  is even smaller for the STD data which is surprising as it is assumed that the uncertainty of the STD processing is higher. This is presumably due to the combination of different products in the E-GVAP ZTD data set which leads to a rather high variability in the processed ZTDs. The STD data are provided by only one processing center and seem to be more consistent. The standard deviation  $\sigma_{\text{map}}$  is in the order of the expected STD error. In an ideal case the STD error is the ZTD error mapped to the

ICON	all	selected
$N_{\text{obs}}$	42163245	41149006
$\bar{\Delta}$ [mm]	25.0	23.9
$\bar{\Delta}_{\text{map}}$ [mm]	10.6	10.1
$\bar{\Delta}_{\text{rel}}$ [%]	0.46	0.44
$\sigma$ [mm]	37.4	33.8
$\sigma_{\text{map}}$ [mm]	12.2	10.8
$\sigma_{\text{rel}}$ [%]	0.55	0.47

Table 2: Verification of STD observations with ICON for March 2015. Bias and standard deviation  $\sigma$  were computed using all data (col. *all*) or selected data with  $\Delta \leq 1.5\%$  (col. *selected*).

signal path but for STD assimilation a larger error should be assumed. Järvinen u. a. (2007) suggest a fit to an empirical mapping function leading to an observation error of  $\sim 12$  mm in zenith direction and  $\sim 95$  mm at an elevation of  $10^\circ$ . Kawabata u. a. (2013) assume a much larger error of 50 mm in zenith direction.

#### 5.4 Validation with COSMO-DE

The same STD data set as in the previous section was used for validating the STD operator with the COSMO-DE. The STD operator was applied to operational hourly COSMO-DE analyses in order to compute the model equivalents of all available STD observations in March 2015. The operator was running in an off-line mode which is comparable to the En-Var passive mode of ICON, i. e. it is applied to hourly model analyses.

The same parameters as in the previous section were computed for COSMO-DE using the data of 161 GNSS stations (tab. 3). The bias  $\bar{\Delta}_{\text{map}} = 5.5$  mm is almost equal to the expected antenna calibration bias in the GFZ data ( $\sim 6$  mm) and much smaller than the bias to ICON. This might indicate a dry bias of ICON of about 5 mm in zenith direction. The standard deviation  $\sigma_{\text{map}} = 10.7$  mm for all data and 10.0 mm for the selected data is slightly better as in case of ICON and rather close to an optimistic estimate of the STD error.

The distribution of  $\Delta$  with respect to the elevation  $\varepsilon$  is shown in fig. 5. Only data with  $\Delta \leq 1.5\%$  were regarded. The distribution is rather narrow

COSMO	all	selected
$N_{\text{obs}}$	22364054	22225645
$\bar{\Delta}$ [mm]	12.9	12.9
$\Delta_{\text{map}}$ [mm]	5.6	5.5
$\Delta_{\text{rel}}$ [%]	0.24	0.24
$\sigma$ [mm]	31.4	29.4
$\sigma_{\text{map}}$ [mm]	10.7	10.0
$\sigma_{\text{rel}}$ [%]	0.51	0.43

Table 3: Verification of STD observations with COSMO-DE for March 2015.  $\bar{\Delta}$  and  $\sigma$  were computed using all data (col. *all*) or selected data with  $\Delta \leq 1.5\%$  (col. *selected*).

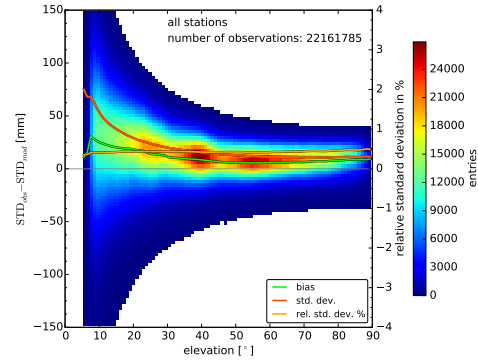


Figure 5: Distribution of  $\Delta$  with the elevation  $\varepsilon$  for COSMO-DE. The variation of the bias (green line, mm) and the standard deviation (red line, mm) with the elevation is shown together with the relative standard deviation (orange line in %, right scale).

at large elevations ( $\sigma \approx 14$  mm) but widens considerably at small elevations ( $\sigma \approx 70$  mm). The standard deviation is increasing accordingly (red line in fig. 5). As the uncertainty of both the observations and their model equivalents increases with decreasing elevation this could be expected. However, the standard deviation increases proportional to the assumed STD error and leads to an almost constant relative error  $\bar{\Delta}_{\text{rel}}$  which seems even to decrease slightly at low elevations (orange line in fig. 5, right scale).

The GFZ STD data set shows a bias (see Sec. 5.4) which is also present in fig. 5, green line. The bias increases at low elevations and leads

to slightly distorted distributions. Within the STD data processing several components of the STD are estimated and some of them are mapped to the slant path (Bender u. a., 2011). If one of these components shows a bias, the bias will also be mapped and increase with decreasing elevation. The bias in fig. 5 shows a minimum near  $\varepsilon = 50^\circ$  which is due to the combination of many different stations. No individual station shows such a behavior. There are some almost bias free stations which show a symmetric nearly Gaussian distribution. The distribution obtained with ICON analyses is very similar but with a somewhat larger bias and standard deviation (tab. 2).

For this validation study almost all GNSS data were used in order to investigate the behavior of the STD operator and to establish a basis for monitoring the GNSS products of different processing centers. For data assimilation a bias correction will be applied and much more rigorous selection criteria will be used leading to a considerably smaller standard deviation of the assimilated GNSS data.

## 6 Conclusions

A slant total delay observation operator for assimilating GNSS STD and ZTD observations was developed at the German Weather Service (DWD). The operator was integrated into the ICON En-Var assimilation system as well as in the COSMO-DE LETKF. In order to assimilate STDs in arbitrary directions and with any desired elevation the operator needs to account for the Earth's curvature and for the signal bending in the atmosphere. The former is achieved by transforming all coordinates into an ellipsoidal reference frame (WGS84) which provides the curvatures in zonal and meridional directions. Geoid corrections are applied if necessary to obtain heights above the ellipsoid. The curved signal path in the atmosphere is estimated by a raytracer based on Fermat's principle and the delays are computed along this curved signal path.

First tests with the STD operator were carried out using four weeks of ICON and COSMO-DE analyses. The operator output was compared with ZTD data provided by E-GVAP and STD data provided by the GFZ in Potsdam.

The results of the comparison are quite promising. In general, the standard deviation of the ob-

servation minus model differences is in the order of the GNSS delay errors, i. e. about 10 mm in zenith direction. The standard deviation of STD observations mapped into zenith direction is comparable to the ZTD standard deviation. In case of ICON the STD standard deviation is even slightly smaller ( $\sigma_{\text{STD}} = 10.8$  mm,  $\sigma_{\text{ZTD}} = 11.9$  mm). Furthermore, the relative STD error seems to be independent of the elevation and it can be assumed that the information provided by STD observations at low elevations is not considerably reduced by the observation error. These results indicate that the model states are already compatible with the GNSS observations and can be further improved by assimilating observations of this kind.

However, there are strong variations between different GNSS processing centers and between individual GNSS stations. The bias as well as the standard deviation differs in most cases even if the same station is regarded. On the other hand there are variations in the quality of individual stations which are seen by all processing centers. The monitoring results are therefore required to set up a quality control for different processing centers and stations. Currently, new strategies are developed for multi GNSS processing and real-time processing and lots of new GNSS products will be available which need to be monitored carefully.

Experiments in a pre-operational cycled assimilation/forecast environment are in progress and show encouraging results. The impact of GNSS observations on the weather forecasts will be investigated and the improvements by ZTD and/or STD assimilation will be compared.

## References

- [Alber u. a. 2000] ALBER, C. ; WARE, R. ; ROCKEN, C. ; BRAUN, J.: Obtaining single path delays from GPS double differences. In: *Geophysical Research Letters* 27 (2000), Nr. 7, S. 2661–2664
- [Aparicio u. Laroche 2011] APARICIO, Josep M. ; LAROCHE, Stéphane: An evaluation of the expression of the atmospheric refractivity for GPS signals. In: *Journal of Geophysical Research* 116 (2011), D11104. [http:](http://)

- [//dx.doi.org/10.1029/2010JD015214](http://dx.doi.org/10.1029/2010JD015214). – DOI 10.1029/2010JD015214
- [Bender u. a. 2011] BENDER, M. ; DICK, G. ; GE, M. ; DENG, Z. ; WICKERT, J. ; KAHLE, Hans-Gert ; RAABE, A. ; TETZLAFF, G.: Development of a GNSS Water Vapor Tomography System Using Algebraic Reconstruction Techniques. In: *Advances in Space Research* 47 (2011), Nr. 10, S. 1704–1720. <http://dx.doi.org/10.1016/j.asr.2010.05.034>. – DOI 10.1016/j.asr.2010.05.034
- [Bender u. a. 2008] BENDER, M. ; DICK, G. ; WICKERT, J. ; SCHMIDT, T. ; SONG, S. ; GENDT, G. ; GE, M. ; ROTHACHER, M.: Validation of GPS Slant Delays using Water Vapour Radiometers and Weather Models. In: *Meteorologische Zeitschrift* 17 (2008), Nr. 6, 807-812. <http://dx.doi.org/10.1127/0941-2948/2008/0341>. – DOI 10.1127/0941-2948/2008/0341
- [Bennitt u. Jupp 2012] BENNITT, Gemma V. ; JUPP, Adrian: Operational Assimilation of GPS Zenith Total Delay Observations into the Met Office Numerical Weather Prediction Models. In: *Monthly Weather Review* 140 (2012), 27062719. <http://dx.doi.org/10.1175/MWR-D-11-00156.1>. – DOI 10.1175/MWR-D-11-00156.1
- [Bevis u. a. 1992] BEVIS, M. ; BUSINGER, S. ; HERRING, T. A. ; ROCKEN, C. ; ANTHES, R. A. ; WARE, R. H.: GPS Meteorology: Remote Sensing of Atmospheric Water Vapor Using the Global Positioning System. In: *Journal of Geophysical Research* 97 (1992), Nr. D14, S. 15787–15801
- [Bevis u. a. 1994] BEVIS, Michael ; BUSINGER, Steven ; CHISWELL, Steven ; HERRING, Thomas A. ; ANTHES, Richard A. ; ROCKEN, Christian ; WARE, Randolph H.: GPS Meteorology: Mapping Zenith Wet Delays onto Precipitable Water. In: *Journal of Applied Meteorology* 33 (1994), Nr. 3, S. 379–386. <http://dx.doi.org/10.1175/1520-0450>. – DOI 10.1175/1520-0450
- [Bi u. a. 2006] BI, Y. M. ; MAO, J. T. ; LIU, X. Y. ; FU, Y. ; LI, C. C.: Remote sensing of the amount of water vapor along the slant path using the ground-base GPS. In: *Chinese Journal of Geophysics-Chinese Edition* 49 (2006), Nr. 2, S. 335–342. – 19
- [Braun u. a. 2001] BRAUN, John ; ROCKEN, Christian ; WARE, Randolph: Validation of line-of-sight water vapor measurements with GPS. In: *Radio Science* 36 (2001), Nr. 3, S. 459–472
- [Courant u. Hilbert 1953] COURANT, Richard ; HILBERT, David: *Methods of Mathematical Physics*. Wiley, 1953
- [Deng u. a. 2011] DENG, Z. ; BENDER, M. ; ZUS, F. ; GE, M. ; DICK, G. ; RAMATSCHI, M. ; WICKERT, J. ; LÖHNERT, U. ; SCHÖN, S.: Validation of tropospheric slant path delays derived from single and dual frequency GPS receivers. In: *Radio Science* 46 (2011), RS6007. <http://dx.doi.org/10.1029/2011RS004687>. – DOI 10.1029/2011RS004687
- [Elgered u. a. 1991] ELGERED, G. ; DAVIS, J. L. ; HERRING, T. A. ; SHAPIRO, I. I.: Geodesy by radio interferometry: Water vapor radiometry for estimation of the wet delay. In: *Journal of Geophysical Research* 96 (1991), Nr. B4, S. 6541–6555
- [Eresmaa u. a. 2007] ERESMAA, R. ; JÄRVINEN, H. ; NIEMELÄ, S. ; SALONEN, K.: Asymmetry of ground-based GPS slant delay data. In: *Atmospheric Chemistry and Physics* 7 (2007), Nr. 12, 3143-3151. <http://www.atmos-chem-phys.net/7/3143/2007/acp-7-3143-2007.html>
- [Eresmaa u. a. 2008] ERESMAA, Reima ; HEALY, Sean ; JÄRVINEN, Heikki ; SALONEN, Kirsti: Implementation of a ray-tracing operator for ground-based GPS Slant Delay observation modeling. In: *Journal of Geophysical Research* 113 (2008), S. D11114. <http://dx.doi.org/10.1029/2007JD009256>. – DOI 10.1029/2007JD009256,
- [Eresmaa u. Järvinen 2006] ERESMAA, Reima ; JÄRVINEN, Heikki: An observation operator for ground-based GPS slant delays. In: *Tellus* 58A (2006), S. 131–140
- [Fernández del Río u. a. 2015] FERNÁNDEZ DEL RÍO, Ana ; CRESS, Alexander ; RHODIN, Andreas ; DENHARD, Michael ; AMBADAN, Jai-son T. ; ANLAUF, Harald ; POTTHAST, Roland:

- Global Ensemble Data Assimilation for ICON*. <http://data-assimilation.jp/isda2015/program/pdf/5-2.pdf>. Version:2015. – 4. International Symposium on Data Assimilation (ISDA), Kobe, Japan
- [Flores u.a. 2000] FLORES, A. ; RUFFINI, G. ; RIUS, A.: 4D tropospheric tomography using GPS slant wet delays. In: *Annales Geophysicae* 18 (2000), Nr. 2, S. 223–234
- [Förste u.a. 2013] FÖRSTE, Christoph ; BRUNSMA, Sean ; MARTY, Jean-Charles ; FLECHTNER, Frank ; ABRIKOSOV, Oleh ; DAHLE, Christoph ; LEMOINE, Jean-Michel ; NEUMAYER, Karl H. ; BIANCALE, Richard ; BARTHELMES, Franz ; KÖNIG, Rolf: EIGEN-6C3stat - the newest High Resolution Global Combined Gravity Field Model based on the 4th Release of the GOCE Direct Approach. Version:2013. <http://icgem.gfz-potsdam.de/ICGEM/documents/Foerste-et-al-EIGEN-6C3stat.pdf>. Potsdam/Toulouse, Sept., 2013. – Talk
- [Gendt u.a. 2004] GENDT, Gerd ; DICK, Galina ; REIGBER, Christoph ; TOMASSINI, Maria ; LIU, Yanxiong ; RAMATSCHI, Markus: Near Real Time GPS Water Vapor Monitoring for Numerical Weather Prediction in Germany. In: *Journal of the Meteorological Society of Japan* 82 (2004), Nr. 1B, S. 361–370
- [Gill u. Miller 1972] GILL, P. E. ; MILLER, G. F.: An algorithm for the integration of unequally spaced data. In: *The Computer Journal* 15 (1972), Nr. 1, 80-83. <http://dx.doi.org/10.1093/comjnl/15.1.80>. – DOI 10.1093/comjnl/15.1.80
- [Guerova u.a. 2016] GUEROVA, Guergana ; JONES, Jonathan ; DOUSAA, Jan ; DICK, Galina ; HAAN, Siebren de ; POTTIAUX, Eric ; BOCK, Olivier ; PACIONE, Rosa ; ELGERED, Gunnar ; VEDEL, Henrik ; BENDER, Michael: Review of the state-of-the-art and future prospects of the ground-based GNSS meteorology in Europe. In: *Atmospheric Chemistry and Physics* (2016)
- [Ha u.a. 2003] HA, So-Young ; KUO, Ying-Hwa ; GUO, Yong-Run ; LIM, Gyu-Ho: Variational Assimilation of Slant-Path Wet Delay Measurements from a Hypothetical Ground-Based GPS Network. Part I: Comparison with Precipitable Water Assimilation. In: *Monthly Weather Review* 131 (2003), Nr. 11, S. 2635–2655
- [de Haan u.a. 2002] HAAN, S. de ; MAREL, H. van d. ; BARLAG, S.: Comparison of GPS slant delay measurements to a numerical model: case study of a cold front passage. In: *Physics and Chemistry of the Earth* 27 (2002), Nr. 4-5, S. 317–322
- [Healy 2011] HEALY, S. B.: Refractivity coefficients used in the assimilation of GPS radio occultation measurements. In: *Journal of Geophysical Research* 116 (2011), D01106. <http://europa.agu.org/?view=article&uri=/journals/jd/jd1101/2010JD014013/2010JD014013.xml&t=jd,Healy>
- [Hofmann-Wellenhop u.a. 2008] HOFMANN-WELLENHOF, Bernhard. ; LICHTENEGGER, Herbert ; WASLE, Elmar: *GNSS Global Navigation Satellite Systems*. Springer, 2008 (548)
- [Järvinen u.a. 2007] JÄRVINEN, Heikki ; ERESMAA, Reima ; VEDEL, Henrik ; SALONEN, Kirsti ; NIEMELÄ, Sami ; VRIES, John de: A variational data assimilation system for ground-based GPS slant delays. In: *Quarterly Journal of the Royal Meteorological Society* 133 (2007), 969980. <http://dx.doi.org/10.1002/qj.79>. – DOI 10.1002/qj.79
- [Kačmařík u.a. 2012] KAČMAŘÍK, Michal ; DOUŠA, Jan ; ZAPLETAL, Jan: Comparison of GPS slant wet delays acquired by different techniques. In: *Acta Geodynamica et Geomaterialia* 9 (2012), Nr. 4, S. 427–433
- [Kawabata u.a. 2011] KAWABATA, Takuya ; KURODA, Tohru ; SEKO, Hiromu ; SAITO, Kazuo: A Cloud-Resolving 4DVAR Assimilation Experiment for a Local Heavy Rainfall Event in the Tokyo Metropolitan Area. In: *Monthly Weather Review* 139 (2011), Nr. 6, 1911-1931. <http://dx.doi.org/10.1175/2011MWR3428.1>. – DOI 10.1175/2011MWR3428.1
- [Kawabata u.a. 2007] KAWABATA, Takuya ; SEKO, Hiromu ; SAITO, Kazuo ; KURODA, Tohru ; TAMIYA, Kyuichiro ; TSUYUKI, Tadashi ; HONDA,

- Yuki ; WAKAZUKI, Yasutaka: An Assimilation and Forecasting Experiment of the Nerima Heavy Rainfall with a Cloud-Resolving Non-hydrostatic 4-Dimensional Variational Data Assimilation System. In: *Journal of the Meteorological Society of Japan* 85 (2007), Nr. 3, 255-276. <http://dx.doi.org/10.2151/jmsj.85.255>. – DOI 10.2151/jmsj.85.255
- [Kawabata u. a. 2013] KAWABATA, Takuya ; SHOJI, Yoshinori ; SEKO, Hiromu ; SAITO, Kazuo: A Numerical Study on a Mesoscale Convective System over a Subtropical Island with 4D-Var Assimilation of GPS Slant Total Delays. In: *Journal of the Meteorological Society of Japan* 91 (2013), Nr. 5, 705-721. <http://dx.doi.org/10.2151/jmsj.2013-510>. – DOI 10.2151/jmsj.2013-510
- [Lemoine u. a. 1998] LEMOINE, F. G. ; KENYON, S. C. ; FACTOR, J. K. ; TRIMMER, R.G. ; PAVLIS, N. K. ; CHINN, D. S. ; COX, C. M. ; KLOSKO, S. M. ; LUTHCKE, S. B. ; TORRENCE, M. H. ; WANG, Y. M. ; WILLIAMSON, R. G. ; PAVLIS, E. C. ; RAPP, R. H. ; OLSON, T. R.: The Development of the Joint NASA GSFC and NIMA Geopotential Model EGM96 / NASA Goddard Space Flight Center. Version:1998. [http://bowie.gsfc.nasa.gov/697/staff/lemoine/EGM96\\_NASA-TP-1998-206861.pdf](http://bowie.gsfc.nasa.gov/697/staff/lemoine/EGM96_NASA-TP-1998-206861.pdf). Greenbelt, Maryland, 20771 US, 1998 (NASA/TP-1998-206861). – NASA Technical Paper
- [Liu u. Xue 2006] LIU, Haixia ; XUE, Ming: Retrieval of Moisture from Slant-Path Water Vapor Observations of a Hypothetical GPS Network Using a Three-Dimensional Variational Scheme with Anisotropic Background Error. In: *Monthly Weather Review* 134 (2006), Nr. 3, S. 933–949
- [Liu u. a. 2007] LIU, Haixia ; XUE, Ming ; PURSER, R. J. ; PARRISH, David F.: Retrieval of Moisture from Simulated GPS Slant-Path Water Vapor Observations Using 3DVAR with Anisotropic Recursive Filters. In: *Monthly Weather Review* 135 (2007), Nr. 4, S. 1506-1521. <http://dx.doi.org/10.1175/MWR3345.1>. – DOI 10.1175/MWR3345.1
- [MacDonald u. a. 2002] MACDONALD, Alexander E. ; XIE, Yuanfu ; WARE, Randolph H.: Diagnosis of Three-Dimensional Water Vapor Using a GPS Network. In: *Monthly Weather Review* 130 (2002), Nr. 2, S. 386–397. <http://dx.doi.org/10.1175/1520-0493>. – DOI 10.1175/1520-0493
- [Mahfouf u. a. 2015] MAHFOUF, Jean-Francois ; AHMED, Furqan ; MOLL, Patrick ; TEFERLE, Felix N.: Assimilation of zenith total delays in the AROME France convective scale model: a recent assessment. In: *Tellus A* 67 (2015), 26106. <http://dx.doi.org/10.3402/tellusa.v67.26106>. – DOI 10.3402/tellusa.v67.26106
- [van der Marel u. Gündlich 2006] MAREL, Hans van d. ; GÜNDLICH, Brigitte: Slant Delay Retrieval and Multipath Mapping Software / Delft University of Technology. 2006. – TOUGH Deliverable D33
- [Nafisi u. a. 2011] NAFISI, Vahab ; URQUHART, Landon ; SANTOS, Marcelo C. ; NIEVINSKI, Felipe G. ; BÖHM, Johannes ; WIJAYA, Dudy D. ; SCHUH, Harald ; ARDALAN, Alireza A. ; HOBIGER, Thomas ; ICHIKAWA, Ryuichi ; ZUS, Florian ; WICKERT, Jens ; GEGOUT, Pascal: Comparison of Ray-Tracing Packages for Troposphere Delays. In: *IEEE Transactions on Geoscience and Remote Sensing* 50 (2011), Nr. 2, S. 469 – 481. <http://dx.doi.org/10.1109/TGRS.2011.2160952>. – DOI 10.1109/TGRS.2011.2160952
- [NOAA 1976] NOAA: U.S. Standard Atmosphere, 1976 / NOAA. Version:1976. [http://ntrs.nasa.gov/archive/nasa/casi.ntrs.nasa.gov/19770009539\\_1977009539.pdf](http://ntrs.nasa.gov/archive/nasa/casi.ntrs.nasa.gov/19770009539_1977009539.pdf). 1976 (NOAA-S/T 76-1562). – Forschungsbericht
- [Notarpietro u. a. 2011] NOTARPIETRO, Riccardo ; CUCCA, Manuela ; GABELLA, Marco ; VENUTI, Giovanna ; PERONA, Giovanni: Tomographic reconstruction of Wet and Total Refractivity fields from GNSS receiver networks. In: *Advances in Space Research* 47 (2011), Nr. 5, 769-912. <http://dx.doi.org/10.1016/j.asr.2010.12.025>. – DOI 10.1016/j.asr.2010.12.025
- [Picone u. a. 2002] PICONE, J. M. ; HEDIN, A. E. ; DROB, D. P. ; AIKIN, A. C.: NRLMSISE-00

- empirical model of the atmosphere: Statistical comparisons and scientific issues. In: *Journal of Geophysical Research* 107 (2002), Nr. A12, S. 1468. <http://dx.doi.org/10.1029/2002JA009430>. – DOI 10.1029/2002JA009430
- [Rocken u. a. 1993] ROCKEN, C. ; WARE, R. H. ; HOVE, T. V. ; SOLHEIM, F. ; ALBER, C. ; JOHNSON, J. ; BEVIS, M. ; BUSINGER, S.: Sensing Atmospheric Water Vapor with the Global Positioning System. In: *Geophysical Research Letters* 20 (1993), Nr. 23, S. 2631–2634
- [Rüeger 2002] RÜEGER, Jean M.: Refractive Index Formulae for Radio Waves. In: *FIG XXII International Congress*, 2002. – FIG XXII International Congress Washington, D.C. USA, April 19-26 2002
- [Saastamoinen 1972] SAASTAMOINEN, J.: Atmospheric correction for the troposphere and stratosphere in radio ranging of satellites. Version: 1972. <http://www.agu.org/cgi-bin/agubooks>. In: HENRIKSEN, S. W. (Hrsg.) ; MANCINI, A. (Hrsg.) ; CHOVIK, B. H. (Hrsg.): *The Use of Artificial Satellites for Geodesy* Bd. 15. American Geophysical Union (AGU), 1972, 247-251
- [Schraff u. a. 2016] SCHRAFF, C. ; REICH, H. ; RHODIN, A. ; SCHOMBURG, A. ; STEPHAN, K. ; PERIÁÑEZ, A. ; POTTHAST, R.: Kilometre-Scale Ensemble Data Assimilation for the COSMO Model (KENDA). In: *Quarterly Journal of the Royal Meteorological Society* (2016). <http://dx.doi.org/10.1002/qj.2748>. – DOI 10.1002/qj.2748
- [Shangguan u. a. 2015] SHANGGUAN, M. ; HEISE, S. ; BENDER, M. ; DICK, G. ; RAMATSCHI, M. ; WICKERT, J.: Validation of GPS atmospheric water vapor with WVR data in satellite tracking mode. In: *Annales Geophysicae* 33 (2015), Nr. 1, 55-61. <http://dx.doi.org/10.5194/angeo-33-55-2015>. – DOI 10.5194/angeo-33-55-2015
- [Smith u. Weintraub 1953] SMITH, E. K. ; WEINTRAUB, S.: The Constants in the Equation for Atmospheric Refractive Index at Radio Frequencies. In: *Proceedings of the I.R.E.* 41 (1953), 1035-1037. [http://ieeexplore.ieee.org/xpl/freeabs\\_all.jsp?arnumber=4051437](http://ieeexplore.ieee.org/xpl/freeabs_all.jsp?arnumber=4051437)
- [Thayer 1974] THAYER, Gordon T.: An improved equation for the radio refractive index of air. In: *Radio Science* 9 (1974), Nr. 10, S. 803–807
- [de Vries 2006] VRIES, J. de: Validation and Error Modelling of GPS Tropospheric Slant Delays / KNMI. 2006. – TOUGH Deliverable 37
- [Ware u. a. 1997] WARE, Randolph ; ALBER, Chris ; ROCKEN, Christian ; SOLHEIM, Fredrick: Sensing Integrated Water Vapor along GPS ray paths. In: *Geophysical Research Letters* 24 (1997), Nr. 4, S. 417–420. <http://dx.doi.org/10.1029/97GL00080>. – DOI 10.1029/97GL00080
- [Xu 2007] XU, Guochang: *GPS – theory, algorithms, and applications*. Springer, 2007
- [Zänagl u. a. 2014] ZÄNGL, Günther ; REINERT, Daniel ; RIPODAS, Pilar ; BALDAUF, Michael: The ICON (ICOsahedral Non-hydrostatic) modelling framework of DWD and MPI-M: Description of the non-hydrostatic dynamical core. In: *Quarterly Journal of the Royal Meteorological Society* (2014). <http://dx.doi.org/10.1002/qj.2378>. – DOI 10.1002/qj.2378
- [Zus u. a. 2012] ZUS, Florian ; BENDER, Michael ; DENG, Zhiguo ; DICK, Galina ; HEISE, Stefan ; SHANG-GUAN, Ming ; WICKERT, Jens: A methodology to compute GPS slant total delays in a numerical weather model. In: *Radio Science* 47 (2012). <http://dx.doi.org/10.1029/2011RS004853>. – DOI 10.1029/2011RS004853
- [Zus u. a. 2013] ZUS, Florian ; DICK, Galina ; DOUSA, Jan ; HEISE, Stefan ; WICKERT, Jens: The rapid and precise computation of GPS slant total delays and mapping factors utilizing a numerical weather model. In: *Radio Science* submitted (2013)